

Automatic Crosswind Flight of Tethered Wings for Airborne Wind Energy: Modeling, Control Design, and Experimental Results

Lorenzo Fagiano, *Member, IEEE*, Aldo U. Zraggen, Manfred Morari, *Fellow, IEEE*,
and Mustafa Khammash, *Fellow, IEEE*

I. INTRODUCTION

AIRBORNE wind energy systems aim at harnessing the wind blowing up to 1000 m above the ground, using tethered wings or aircrafts. In recent years, an increasing number of researchers in academia and industry started to investigate this idea (see [1]–[12] as well as [13] for an overview).

In several concepts that are currently being developed, a tethered flexible wing has to be controlled to fly in crosswind conditions, i.e., roughly perpendicular to the wind flow [14], and the traction forces acting on the lines are converted into electricity using mechanical and electrical equipments installed on the ground [2], [5], [6], [11]. The automatic control of the wing is a key aspect of airborne wind energy. When energy is produced, the aim is to make the wing fly along figure-eight paths, which yield the highest traction forces while preventing line twisting. This control problem involves fast, nonlinear, unstable time-varying dynamics subject to hard operational constraints, and external disturbances. Contributions by various research groups and companies worldwide have recently appeared in the literature, e.g., [8], [9], [11], [15]–[17]. Most of the presented approaches [7]–[9], [15], [18], implemented in numerical simulations only, are based on a nonlinear point-mass model of the system, derived on the basis of first-principle laws of mechanics and aerodynamics, and they rely on the use of advanced nonlinear control design techniques, including either tracking [8] or economic [9] model predictive control and adaptive control-Lyapunov techniques [11]. However, the use of these approaches in a real system appears to be not trivial, due to the discrepancies between the employed simplified model and the real dynamics of flexible wings, the need to solve complex nonlinear optimization problems in real time, finally the need to measure the wind speed and direction at the wing's flying altitude.

In contrast with the mentioned works, in a recent contribution, concerned with the control of large kites for seagoing vessels [17], a simpler dynamical model has been proposed and used for control design. Such a model has been justified through measured data, and the designed control system has been tested experimentally, thus showing the practical applicability of the approach. It has to be noted that a similar model has been considered also in [11], where it has been justified by *a priori* assumptions. Hence, neither [11] nor [17] provided an explicit link between the model considered in the control design and the wing's characteristics, such as area, efficiency, and mass. The approach proposed in [17] is composed by an inner control loop that computes the input needed to obtain a desired reference heading of the wing, and an outer control loop that computes the reference heading

Manuscript received January 4, 2013; revised June 24, 2013; accepted August 20, 2013. Manuscript received in final form August 22, 2013. Date of publication September 10, 2013; date of current version June 16, 2014. This work was supported in part by the California Energy Commission under EISG Grant 56983A/10-15, "Autonomous Flexible Wings for High-Altitude Wind Energy Generation," and in part by the European Union Seventh Framework Programme (FP7/2007-2013) under Grant Agreement PEOF-GA-2009-252284 – Marie Curie Project "Innovative Control, Identification and Estimation Methodologies for Sustainable Energy Technologies." Recommended by Associate Editor J. Y. Lew.

L. Fagiano is with the Automatic Control Laboratory, Swiss Federal Institute of Technology, Zurich 8092, Switzerland, and also with the Department of Mechanical Engineering, University of California, Santa Barbara, CA 93105 USA (e-mail: lorenzo.fagiano@gmail.com).

A. U. Zraggen and M. Morari are with the Automatic Control Laboratory, Swiss Federal Institute of Technology, Zurich 8092, Switzerland (e-mail: zraggen@control.ee.ethz.ch; morari@control.ee.ethz.ch).

M. Khammash is with the Department of Biosystems Science and Engineering, ETH Zurich 8903, Switzerland (e-mail: mustafa.khammash@bse.ethz.ch).

Color versions of one or more of the figures in this paper are available online.

according to a bang-bang-like strategy. The inner control loop is a quite sophisticated model following approach and it needs the measure of the apparent wind speed at the wing's altitude, obtained from an onboard anemometer.

In the described context, we present here new contributions in the field of control of flexible tethered wings for airborne wind energy systems with ground-level generators. We focus on the problem of controlling the wing to achieve figure-eight crosswind paths. First, we consider a simplified model based on the notion of “velocity angle” of the wing, similar in form to the one proposed in [11] and [17], and we derive an explicit link between the model's parameters and the system's characteristics. We show the validity of such a model as compared with experimental data collected with a small-scale prototype. This result provides a definitive assessment of the considered control-oriented model for tethered wings, thus bridging the gap between theoretical equations and experimental evidence. As a second contribution, we present a new control algorithm for tethered wings, based on the derived simplified model. Differently from [8], [11], and [15], the approach does not employ precomputed paths based on a mathematical model of the system, thus avoiding issues related to model mismatch and to the actual feasibility of the employed reference path for the (uncertain and time-varying) dynamics of a real system. In addition, an estimate or measure of the wind speed at the wing's location, as considered in [8], [9], and [15], is not needed, nor is a measure of the apparent wind speed aligned with the wing's longitudinal body axis, used in [17], but only a rough estimate of the wind direction with respect to the ground. We employ a hierarchical structure similar to that of [17], but the controllers employed for the inner and outer control loops are different. In particular, the inner controller is a simple static gain, while the outer one is given by a switching strategy based on the wing's position. The proposed control approach involves few parameters, that can be tuned in an intuitive way. Through exploiting the above-mentioned results pertaining to the control-oriented model, we assess the robustness of the inner control loop analytically, against a wide range of operating conditions in terms of wind speed and wing characteristics. We then present the experimental results obtained by testing the approach on a small-scale prototype realized at the University of California, Santa Barbara, CA, USA, in different wind conditions and using different wings. This paper is organized as follows. Section II describes the considered layout and the derivation of the simplified model for the velocity angle dynamics. The control design is presented in Section III, and experimental results are given in Section IV. A final discussion and future research directions are included in Section V.

II. SYSTEM DESCRIPTION AND MODEL EQUATIONS

A. System Layout

We consider a flexible wing, or power kite, connected by three lines to a ground unit (GU). This setup corresponds to a prototype built at the University of California, Santa Barbara, shown in Fig. 1. In normal flight conditions, the wing's trajectory evolves downwind with respect to the GU.



Fig. 1. Small-scale prototype built at the University of California, Santa Barbara, to research the control of tethered wings for airborne wind energy.

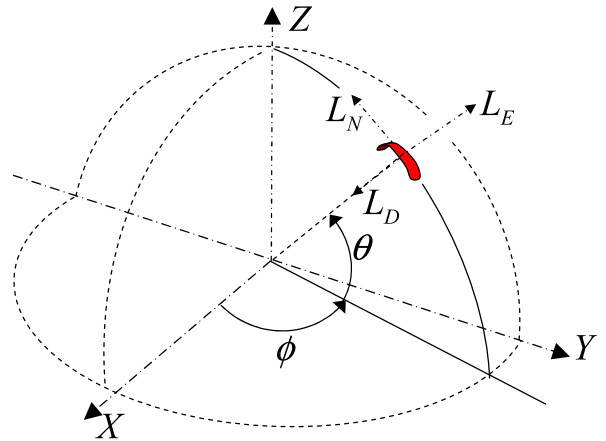


Fig. 2. Reference system $G = (x, y, z)$, wind window (dashed lines), variables θ , ϕ , and local north, east, and down (L_N , L_E , L_D) axes.

For simplicity, we assume that the nominal wind direction (i.e., neglecting turbulence) is aligned with the longitudinal symmetry axis of the GU, denoted by x . This condition can be achieved by properly orienting the GU, exploiting a measure, or estimate of the nominal wind direction. With this assumption in mind, our control approach employs the feedback of the wing's position relative to the GU to obtain crosswind trajectories, i.e., flying paths that are downwind and symmetric with respect to x -axis (i.e., the wind direction). From our experimental results, it turns out that misalignments of about $\pm 30^\circ$ between the wind and the GU do not change significantly the obtained paths relative to the GU, but indeed give place to lower forces on the lines, as expected from the theory (e.g., [16]). The x -axis, together with the z -axis being perpendicular to the ground and pointing upward and with the y -axis to complete a right-handed system, forms the inertial frame $G \doteq (x, y, z)$, centered at the GU (Fig. 2). Through considering a fixed length of the lines, denoted by r , the wing's trajectory is thus confined on a quarter sphere,

given by the intersection of a sphere of radius r centered at the GUs location and the planes $(x, y, z) \in \mathbb{R}^3 : x \geq 0$ and $z \geq 0$. Such a quarter sphere is commonly named “wind window,” Fig. 2 (dashed lines).

Of the three lines connecting the wing to the GU, the two lateral ones, named steering lines, are linked to the back tips of the wing (Fig. 1) and they are used to influence its trajectory: a shorter left steering line with respect to the right one impresses a left turn to the wing (i.e., a counter-clockwise turn as seen from the GU), and viceversa. The center line, named power line, splits into two lines connected to the front of the wing (or leading edge) and sustains $\sim 70\%$ of the generated load. The GU is designed to support the forces acting on the lines and it is equipped with actuators, able to achieve a desired difference of steering lines length. In the considered prototype, a single motor, together with a linear motion system (visible in the lower left corner of Fig. 1), is able to change the difference of length of the steering lines.

In this paper, we focus on the problem of designing a controller able to achieve figure-eight crosswind paths, which maximize the generated forces. The use of a fixed lines’ length does not limit the significance of our results, since the problem of crosswind path control can be decoupled from the problem of controlling the lines’ reeling. Indeed it has been shown that the optimal operation of ground-based airborne wind energy generators is achieved with a constant line speed (equal to approximately one third of the wind speed to maximize power production, e.g., [16]). The settings considered here can be seen as a particular case of constant line speed, equal to zero. Other approaches in the literature follow a similar strategy of using two separate control systems, one for the wing guidance and one for the line unrolling (e.g., [9], [11], [17]). Rather, the use of short lines ($r = 30$ m in our case) makes the control problem more challenging, since the flight paths must be contained in a small area, to avoid contact with the ground or aerodynamic stall occurring at the border of the wind window.

The wing is equipped with onboard sensors and a radio transmitter; the receiver and other sensors are installed on the GU. These sensors, together with suitable filtering algorithms, provide accurate real-time estimates of the wing’s position and velocity vector, to be used for feedback control. For the sake of simplicity, in this paper the feedback variables are considered to be available for the control computation; the interested reader is referred to [19] for details on the estimation approach that we used. In the next section, we briefly recall a point-mass dynamical model of the system and introduce the notion of velocity angle of the wing. The latter is one of the feedback variables we use and it represents a novelty with respect to the mentioned previous approaches.

B. Model Equations

We consider the point-mass model already employed in previous contributions (e.g., [8], [9], [11], [20] and references therein) and adapt it to a slightly different reference system, to introduce the wing’s velocity angle. For the sake of completeness, we recall here the main equations of the point-mass model, since they are instrumental to prove

a theoretical result concerned with the steering dynamics of tethered wings. Through considering the fixed line length r , the wing’s position can be expressed in the inertial frame G using the spherical coordinates $\theta(t)$, $\phi(t)$ as (Fig. 2)

$${}_G\vec{p}(t) = \begin{pmatrix} r \cos(\phi(t)) \cos(\theta(t)) \\ r \sin(\phi(t)) \cos(\theta(t)) \\ r \sin(\theta(t)) \end{pmatrix} \quad (1)$$

where t is the continuous time variable. In (1) and throughout this paper, the subscript letter in front of vectors [e.g., ${}_G\vec{p}(t)$] denotes the reference system considered to express the vector components.

We define also a noninertial coordinate system $L \doteq (L_N, L_E, L_D)$, centered at the wing’s position (also shown in Fig. 2). The L_N axis, or local north, is tangent to the wind window and points toward its zenith. The L_D axis, called local down, points to the center of the sphere (i.e., the GU), hence it is perpendicular to the tangent plane to the wind window at the wing’s location. The L_E axis, named local east, forms a right hand system and spans the tangent plane together with L_N . We note that the system L is a function of the wing’s position only, and it is different from the local systems used in previous researches (e.g., [9] and the references therein), due to the different definition of angle θ . A vector in the L system can be expressed in the G system through the following rotation matrix:

$$R = \begin{pmatrix} -\cos(\phi(t)) \sin(\theta(t)) - \sin(\phi(t)) & -\cos(\phi(t)) \cos(\theta(t)) \\ -\sin(\phi(t)) \sin(\theta(t)) \cos(\phi(t)) & -\sin(\phi(t)) \cos(\theta(t)) \\ \cos(\theta(t)) & 0 & -\sin(\theta(t)) \end{pmatrix}$$

Through applying Newton’s law of motion to the wing in the reference L we obtain

$$\ddot{\theta}(t) = \frac{{}_L\vec{F}(t) \cdot \vec{e}_{L_N}(t)}{rm} - \sin(\theta(t)) \cos(\theta(t)) \dot{\phi}^2(t) \quad (2)$$

$$\ddot{\phi}(t) = \frac{{}_L\vec{F}(t) \cdot \vec{e}_{L_E}(t)}{rm \cos(\theta(t))} + 2 \tan(\theta(t)) \dot{\theta}(t) \dot{\phi}(t) \quad (3)$$

where m is the mass of the wing. In (2)–(3) and throughout this paper we denote unit vectors by “ \vec{e} ” followed by a subscript indicating the related axis, e.g., $\vec{e}_{L_N}(t)$ denotes the unit vector of the L_N axis. The force ${}_L\vec{F}(t)$ consists of contributions from the gravity force ${}_L\vec{F}_g(t)$, the aerodynamic force ${}_L\vec{F}_a(t)$, and the force exerted by the lines, ${}_L\vec{F}_c(t)$. The latter is determined by the balance of all the other forces projected on the line direction. Vector ${}_L\vec{F}_g(t)$ can be computed as

$${}_L\vec{F}_g(t) = \begin{pmatrix} -mg \cos(\theta(t)) \\ 0 \\ mg \sin(\theta(t)) \end{pmatrix} \quad (4)$$

where g is the gravity acceleration. The aerodynamic force is given by the contributions of the lift and drag generated by the wing and of the drag induced by the lines. These forces depend on the apparent wind, $\vec{W}_a(t)$, computed as

$$\vec{W}_a(t) = \vec{W}(t) - \vec{v}(t) \quad (5)$$

where $\vec{W}(t)$ is the wind relative to the ground and $\vec{v}(t) \doteq d\vec{p}/dt$ is the wing velocity vector, which can

be expressed in the L frame as

$${}_L\vec{v}(t) = \begin{pmatrix} r\dot{\theta}(t) \\ r \cos(\theta(t))\dot{\phi}(t) \\ 0 \end{pmatrix}. \quad (6)$$

Then, the aerodynamic force ${}_L\vec{F}_a(t)$ can be computed as (e.g., [9])

$$\vec{F}_a(t) = \frac{1}{2}\rho C_L(t)A|\vec{W}_a(t)|^2\vec{z}_w(t) \quad (7a)$$

$$+ \frac{1}{2}\rho C_D(t)A|\vec{W}_a(t)|^2\vec{x}_w(t) \quad (7b)$$

$$+ \frac{1}{8}\rho C_{D,l}A_l \cos(\Delta\alpha(t))|\vec{W}_a(t)|^2\vec{x}_w(t) \quad (7c)$$

$$\begin{aligned} &= \frac{1}{2}\rho C_L(t)A|\vec{W}_a(t)|^2\vec{z}_w(t) \\ &+ \frac{1}{2}\rho \underbrace{\left(C_D(t) + \frac{C_{D,l}A_l \cos(\Delta\alpha(t))}{4A} \right)}_{C_{D,eq}(t)} \\ &\times A|\vec{W}_a(t)|^2\vec{x}_w(t). \end{aligned} \quad (7d)$$

In (7), the contributions (7a)–(7b) are, respectively, the lift and drag forces generated by the wing, while (7c) is the drag induced by the lines. $C_L(t)$ and $C_D(t)$ are the aerodynamic lift and drag coefficients of the wing, $C_{D,l}$ is the drag coefficient of the lines, A is the reference area of the wing, A_l is the reference area of the lines, ρ is the air density, and $\vec{x}_w(t)$ and $\vec{z}_w(t)$ are the directions of the drag and lift forces, respectively. The parameter $C_{D,eq}(t)$ is called the equivalent aerodynamic drag coefficient, since it accounts for the drag of both the wing and the lines. We note that the aerodynamic coefficients are considered as time-varying parameters here, since they depend on the wing’s angle of attack, which in turn changes in time as a function of the flight conditions. The variable $\Delta\alpha(t)$ is the angle between the apparent wind vector $\vec{W}_a(t)$ and the tangent plane to the wind window at the wing’s location. The vectors $\vec{x}_w(t)$ and $\vec{z}_w(t)$, defining the directions of the lift and drag forces, depend on the direction of the apparent wind and on the roll angle $\psi(t)$ of the wing. In particular, $\vec{x}_w(t)$ points in the direction of the apparent wind $\vec{W}_a(t)$, while $\vec{z}_w(t)$ is perpendicular to $\vec{x}_w(t)$ and to a further vector, denoted by $\vec{e}_l(t)$, which points from the right tip of the wing to the left one, as seen from the GU (e.g., [9] for a formal definition).

Vectors $\vec{x}_w(t)$ and $\vec{z}_w(t)$ can be expressed in the L frame as

$$\begin{aligned} {}_L\vec{x}_w(t) &= \begin{pmatrix} -\cos(\xi(t)) & -\sin(\xi(t)) & 0 \\ -\sin(\xi(t)) & \cos(\xi(t)) & 0 \\ 0 & 0 & -1 \end{pmatrix} \cdot \begin{pmatrix} \cos(\Delta\alpha(t)) \\ 0 \\ \sin(\Delta\alpha(t)) \end{pmatrix} \\ {}_L\vec{z}_w(t) &= \begin{pmatrix} -\cos(\xi(t)) & -\sin(\xi(t)) & 0 \\ -\sin(\xi(t)) & \cos(\xi(t)) & 0 \\ 0 & 0 & -1 \end{pmatrix} \\ &\cdot \begin{pmatrix} -\cos(\psi(t))\cos(\eta(t))\sin(\Delta\alpha(t)) \\ \cos(\psi(t))\sin(\eta(t))\sin(\Delta\alpha(t)) + \sin(\psi(t))\cos(\Delta\alpha(t)) \\ \cos(\psi(t))\cos(\eta(t))\cos(\Delta\alpha(t)) \end{pmatrix}. \end{aligned} \quad (8)$$

In (8), $\eta(t)$ is given by (e.g., [21])

$$\eta(t) = \arcsin(\tan(\Delta\alpha(t))\tan(\psi(t))) \quad (9)$$

and $\psi(t)$ is a function of the steering input, $\delta(t)$

$$\psi(t) = \arcsin\left(\frac{\delta(t)}{d_s}\right) \quad (10)$$

where d_s is the wing span. Finally, $\xi(t)$ is the heading angle of the wing, and it is computed as the angle between the local north L_N and the apparent wind $\vec{W}_a(t)$ projected on the (L_N, L_E) plane

$$\xi(t) = \arctan\left(\frac{\vec{W}_a(t) \cdot \vec{e}_{L_E}(t)}{\vec{W}_a(t) \cdot \vec{e}_{L_N}(t)}\right). \quad (11)$$

In (11), the four-quadrant version of the arc tangent function shall be used, such that $\xi(t) \in [-\pi, \pi]$. The assumption underlying (11) is that the wing’s longitudinal body axis is always contained in the plane spanned by vectors $\vec{W}_a(t)$ and $\vec{p}(t)$. Equations (2)–(11) give an analytic expression for the point-mass model of the wing, with four states $[\theta(t), \phi(t), \dot{\theta}(t), \dot{\phi}(t)]$, one manipulated input $[\delta(t)]$, and three exogenous inputs [the components of vector $\vec{W}(t)$]. Such a model has been widely used in the literature on control design for airborne wind energy applications, e.g., [7]–[9], [11]. In Section II-D we show how a simpler model, which we will use for our control design, can be derived from the dynamics (2)–(11). The variable involved in such control-oriented model is the velocity angle $\gamma(t)$ of the wing, defined as

$$\gamma(t) \doteq \arctan\left(\frac{\vec{v}(t) \cdot \vec{e}_{L_E}(t)}{\vec{v}(t) \cdot \vec{e}_{L_N}(t)}\right) = \arctan\left(\frac{\cos(\theta(t))\dot{\phi}(t)}{\dot{\theta}(t)}\right). \quad (12)$$

The angle $\gamma(t)$ is thus the angle between the local north $\vec{e}_{L_N}(t)$ and the wing’s velocity vector $\vec{v}(t)$. This variable is particularly suited for feedback control, since it describes the flight conditions of the wing with just one scalar, e.g., if $\gamma = 0$ the wing is moving upward toward the zenith of sphere, while $\gamma = \pi/2$ indicates that the wing is moving parallel to the ground toward the local east. In addition, the time derivative $\dot{\gamma}$ defines how fast the wing is being steered while flying in the wind window. Similarly to (11), also in (12) the four-quadrant version of the arc tangent function shall be used, such that $\gamma(t) \in [-\pi, \pi]$.

C. Input Model

The prototype used for our test flights features two attachment points for the steering lines on the GU, left and right. These attachment points are separated by a distance d (Fig. 1, in the lower part, where the attachment points with swaying pulleys are visible). When the wing’s lines are not aligned with the x -axis, this distance induces an equivalent steering deviation. We call such deviation “geometric input”, δ_g , since its value depends on the geometry of the attachment points and on the (θ, ϕ) position of the wing in the wind window. Hence, the overall steering input acting on the wing is

$$\delta(t) = \delta_u(t) + \delta_g(t) \quad (13)$$

where $\delta_u(t)$ is the input issued by the control system, i.e., the difference of length of the steering lines (right minus left) obtained by changing the position of the linear motion system

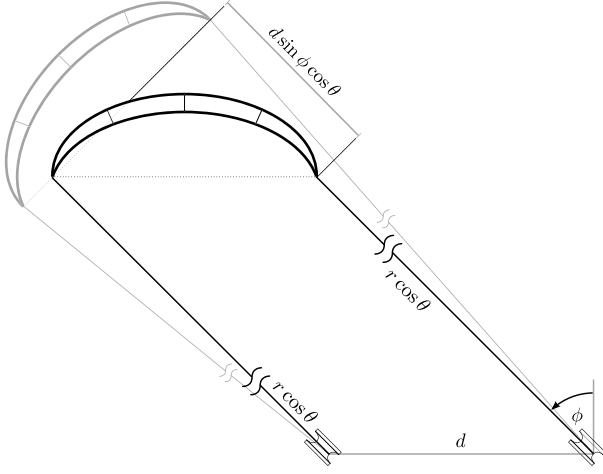


Fig. 3. Sketch of the wing in a generic (θ, ϕ) position as seen from above and related geometric input $\delta_g = d \sin(\phi) \cos(\theta)$.

on the GU. In this section, we derive an expression to compute the geometric input as a function of $\theta(t)$, $\phi(t)$, and d . To this end, we consider the GU and the wing as seen from above, such that the trace of the wind window at the wing's height is a semicircle of radius $r \cos(\theta)$. Let the wing be in a situation in which both tips lie on the tangent plane to the wind window at the current wing position (θ, ϕ) . Since the steering of the wing is essentially induced by a roll motion, by which the wing tips are moved away from the tangent plane, we call this orientation "neutral configuration" (Fig. 3, gray drawing). Now, assuming that $\delta_u = 0$, the left and right lines have the same length, so that if $\phi \neq 0$ the wing tips are forced to leave the neutral configuration (Fig. 3, black drawing), in the same way as a steering input were acting on the wing. In other words, in order for the wing to be in a neutral configuration in the presence of a value of $\phi \neq 0$, the two steering lines should have a difference of length equal to $d \sin(\phi) \cos(\theta)$. Hence, we can compute the geometric input as

$$\delta_g(t) = -d \sin(\phi(t)) \cos(\theta(t)). \quad (14)$$

We note that this quantity is always bounded by d , moreover with increasing θ its value decreases and becomes eventually zero if the wing is at the zenith of the wind window. The minus sign in (14) derives from the fact that the geometric input imposes a counter-clockwise turn (as seen from the GU) for $\phi < 0$ (i.e., $\dot{\gamma} > 0$) and a clockwise turn for $\phi > 0$ (i.e., $\dot{\gamma} < 0$).

D. Control-Oriented Model for Tethered Wings

In [17], a simple model was presented and used for the control design, where the time derivative of the heading angle of the wing is given as a function of the control variable. Here, we consider a similar simplified model, where we use the velocity angle instead of the heading angle. This choice is supported by the assumption of small sideslip angle, as formally stated below.

Assumption 1: The difference between the velocity angle $\gamma(t)$ and the heading angle $\zeta(t)$ is negligible, i.e., the apparent

wind projected onto the tangent plane to the wind window at the wing's location is equal to the wing's velocity $\vec{v}(t)$. In addition, all the forces in the direction of vector $\vec{v}(t)$ are negligible as compared with lift and drag.

Assumption 1 is common in the analysis of airborne wind energy generators (e.g., [14], [16]) and it is reasonable whenever the wing is flying downwind roughly perpendicularly to the wind flow. Indeed in our flight tests, the velocity angle and the wing's heading never differed more than 0.15 rad in crosswind conditions.

With Assumption 1 in mind, the model proposed in [17] can be written in the following form:

$$\dot{\gamma}(t) \simeq \tilde{K}(t)\delta(t) + \tilde{T}(t). \quad (15)$$

In particular, in [17] the term $\tilde{K}(t)$ is given by a constant gain, g_K , multiplied by the magnitude of the apparent wind speed aligned with the wing's heading. Such a model was justified mainly through experimental results in [17], where the gain g_K was derived empirically. In [11], a model of the form (15) is also used, and justified by some assumptions. Equation (15) provides indeed a model well suited for control design, with the right balance between accuracy and simplicity, however neither [17] nor [11] derived an explicit relationship between the model's parameters and the main characteristics of the system, such as wing size, mass, or efficiency. The theoretical result we are presenting next is aimed to fill this gap, by linking (15) to the first-principle model recalled in Section II-B. We consider the following assumption on the roll angle $\psi(t)$.

Assumption 2: The angle $\psi(t)$ is sufficiently small to linearize its trigonometric functions.

Assumption 2 is reasonable in the considered context, since for example the prototype at the UC Santa Barbara operates with $\psi \simeq \pm 7.5^\circ$ (for a 12-m² wing with wingspan $d_s = 3.1$ m) up to $\psi \simeq \pm 12.8^\circ$ (for a 6-m² wing with wingspan $d_s = 1.8$ m). We can now state our theoretical result.

Proposition 1: Let assumptions 1–2 hold. Then, (15) holds with

$$\tilde{K}(t) = \frac{\rho C_L(t) A}{2md_s} \left(1 + \frac{1}{E_{\text{eq}}^2(t)}\right)^2 |\vec{v}(t)| \quad (16a)$$

$$\tilde{T}(t) = \frac{g \cos(\theta(t)) \sin(\gamma(t))}{|\vec{v}(t)|} + \sin(\theta(t)) \dot{\phi}(t) \quad (16b)$$

where $|\vec{v}(t)|$ is the magnitude of the wing's velocity and $E_{\text{eq}}(t) \doteq C_L(t)/C_{D,\text{eq}}(t)$.

Proof: Appendix. ■

Proposition 1 provides an explicit link between the main lumped parameters of the wing, such as area, mass and lift coefficient, and the gain and external disturbance of (15). It is worth elaborating more on this result and its implications. According to (15), there is basically an integrator between the control input $\delta(t)$ and the velocity angle $\gamma(t)$, with a time-varying gain. On the basis of (16a), such a gain increases linearly with the wing's speed: thus, a larger speed provides higher control authority but it can also bring forth stability issues, if the control system is not properly designed. For a given wing flying in crosswind conditions,

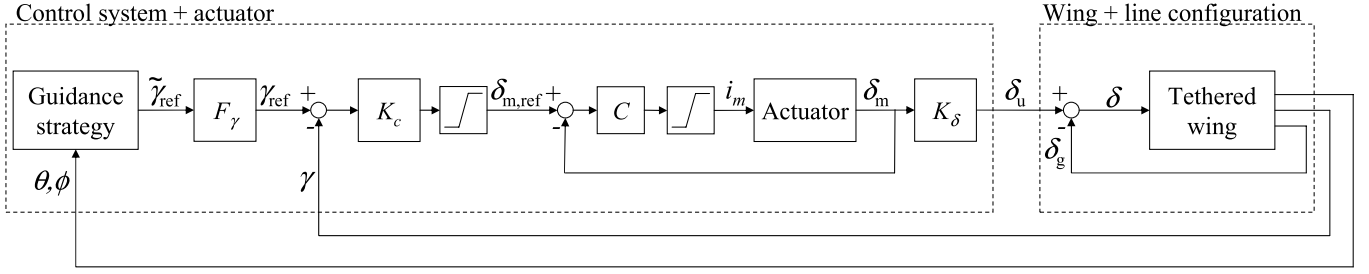


Fig. 4. Overview of the proposed control system.

the term $\rho C_L(t) A / (2md_s) (1 + 1/E_{\text{eq}}^2(t))^2$ does not change significantly during operation, hence supporting the model proposed by [17], where, as mentioned above, a constant gain g_K , multiplied by the apparent wind speed, is used to compute \tilde{K} . Equation (16a) also implies that a larger area-to-mass ratio, A/m , gives in general a higher gain \tilde{K} , and that the steering gain of wings with similar aerodynamic coefficients but different sizes should not change much, provided that they have similar A/m . However, the latter remark holds true if only the wing is considered, while the situation changes if the up-scaling of the lines is also considered, e.g., the use of larger wings would require lines with larger diameter, and the consequent added mass and induced drag would generally reduce both the equivalent efficiency and the A/m .

Since the wing's speed is roughly proportional to the apparent wind speed projected along the lines' direction (e.g., [16]), the gain \tilde{K} can be also rewritten as (assuming that the wind is aligned with the x -axis, as we remarked in Section II-A)

$$\tilde{K}(t) = \frac{\rho C_L(t) A E_{\text{eq}}(t) \cos(\theta(t)) \cos(\phi(t))}{2md_s} \times \left(1 + \frac{1}{E_{\text{eq}}^2(t)}\right)^2 |\vec{W}|. \quad (17)$$

According to (17), the value of \tilde{K} is highest when the wing is flying crosswind, and it decreases as the wing approaches the borders of the wind window (i.e., $\theta \simeq \pi/2$ and/or $\phi \simeq \pm\pi/2$). Therefore, maneuvering the wing in these conditions requires larger control inputs and in some situations it might be not possible, leading to a complete loss of controllability. Similarly, the presence of nonzero reeling speed can be assimilated to a change of wind speed in the line direction, so that the value of $|\vec{v}(t)|$ (and, consequently, of the steering gain \tilde{K}), increases during reel-in and decreases during reel-out. Finally, the wing's efficiency and lift coefficients also play an important role; in particular, for a fixed drag coefficient the gain is expected to grow quadratically with the lift coefficient, as it can be noted from (17) by considering that $E_{\text{eq}} = C_L/C_{D,\text{eq}}$. The term $\tilde{T}(t)$ accounts for the steering effect that the gravity and apparent forces have on the wing. It can be noted that the influence of gravity gets smaller with larger wing speed; hence, it can be easily dominated by the control action during crosswind flight, while it becomes more and more important as the wing moves to the side of the wind window.

As a final remark, we note that (16) can be further refined to also consider the current wing heading with respect to the absolute wind. However, such details would increase significantly the complexity of the equations without adding much value to the result.

We show a comparison between Proposition 1 and experimental data in Section IV-A. In the next section, we introduce a new control approach for crosswind flight of tethered wings, based on the presented simplified model.

III. CONTROL DESIGN

We propose a hierarchical control scheme, shown in Fig. 4. The outer control loop employs the current wing position, in terms of θ, ϕ angles, to compute a reference velocity angle, γ_{ref} , for the middle control loop. The latter employs γ as feedback variable and it has the objective of tracking γ_{ref} , by setting a suitable position reference, $\delta_{m,\text{ref}}$, for the actuator installed on the GU. The innermost control loop then employs a feedback of the motor position δ_m to command the motor's current i_m , to track the desired position $\delta_{m,\text{ref}}$. This control structure allows to separate the nonlinear part of the controller, which is all kept at the outermost level, from the linear one, hence obtaining two simple controllers for the middle and inner loops, for which we can carry out a theoretical robustness analysis. The control algorithm for the outer loop is given by a quite simple guidance strategy, hence making the whole control system very suitable for implementation and experimental testing. In the next sections, we describe each control loop in details. We first adopt a general notation for the involved design parameters and we then provide in Section IV the specific numerical values employed in our tests.

A. Position Control Loop

The innermost loop consists of a standard position control system with an electrical dc brushed motor and a linear motion system, based on a lead screw mechanism. Through neglecting high-order effects, in the absence of external disturbances the dynamics of the actuator can be modeled as

$$\frac{\ddot{\delta}_m(t)}{\omega_m} = -\dot{\delta}_m(t) + K_m i_m(t) \quad (18)$$

where $\delta_m(t)$ is the actuator's position in meters, K_m, ω_m are parameters depending on the actuator's characteristics, and $i_m(t)$ is the commanded current in amperes. In addition, the prototype is equipped with a series of pulleys such that,

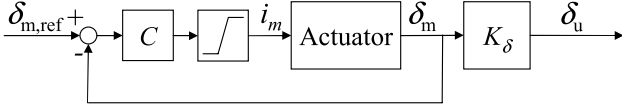


Fig. 5. Scheme of the actuator position control loop.

for a given value of δ_m , the corresponding difference of length of the steering lines is equal to

$$\delta_u(t) = K_\delta \delta_m(t) \quad (19)$$

with K_δ being a known, constant gain. The value of δ_m is measured with high accuracy by an optical rotary incremental encoder, suitably scaled to obtain the linear position of the actuator from the motor's angular position. We use standard loop-shaping control design techniques (e.g., [22]) to design a cascade feedback controller C for this control level. The control scheme is shown in Fig. 5. We note that the actuator has current limits of $\pm \bar{i}_m$, included as a saturation in Fig. 5. Such a saturation does not give rise to integrator windup problems, since the employed controller C does not have integral action. Yet, the presence of an integrator in the plant (18) still yields a closed-loop transfer function with unitary gain between the reference and the output. In particular, the closed loop system for the inner loop results to be in the form

$$\ddot{\delta}_m(t) + 2\zeta_{cl}\omega_{cl}\dot{\delta}_m(t) + \omega_{cl}^2\delta_m(t) = \omega_{cl}^2\delta_{m,\text{ref}}(t) \quad (20)$$

where $\delta_{m,\text{ref}}(t)$ is the reference position provided by the controller for the wing's velocity angle, which is described next.

B. Velocity Angle Control Loop

The control design for the middle loop exploits the model (16). The manipulated variable is the actuator position $\delta_{m,\text{ref}}(t)$ (i.e., the reference for the inner control loop described in Section III-A), and the feedback variable is the wing's velocity angle $\gamma(t)$. The controller is given by a simple proportional law

$$\delta_{m,\text{ref}}(t) = K_c (\gamma_{\text{ref}}(t) - \gamma(t)) \quad (21)$$

where $\gamma_{\text{ref}}(t)$ is the target velocity angle provided by the outer control loop, and K_c is a scalar. The value of K_c is the only design parameter for the velocity angle controller, and it can be tuned at first using (15)–(16a) with some nominal system parameters, and then via experiments. In addition, we show that K_c can be tuned to robustly stabilize the control loop. To this end, we rewrite the dynamical system given by (16a)–(19) and (20)–(21) by considering the velocity angle tracking error

$$\begin{aligned} \Delta_\gamma(t) &\doteq \gamma_{\text{ref}}(t) - \gamma(t) \\ \begin{bmatrix} \dot{\Delta}_\gamma(t) \\ \dot{\delta}_m(t) \\ \dot{\delta}_m(t) \end{bmatrix} &= \underbrace{\begin{bmatrix} 0 & -\tilde{K}(t)K_\delta & 0 \\ 0 & 0 & 1 \\ K_c\omega_{cl}^2 & -\omega_{cl}^2 & -2\zeta_{cl} \end{bmatrix}}_{A_{cl}(\tilde{K}(t))} \begin{bmatrix} \Delta_\gamma(t) \\ \delta_m(t) \\ \dot{\delta}_m(t) \end{bmatrix} + w(t). \end{aligned} \quad (22)$$

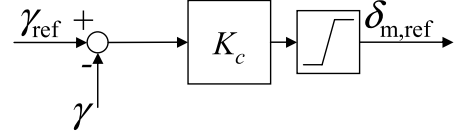


Fig. 6. Scheme of the velocity angle controller.

In (22), the term $\tilde{K}(t)$ corresponds to the gain in (16a) and depends on the system's parameters as well as the wind and flight conditions. The term $w(t)$ accounts for the effects of gravity and apparent forces of (16a), of the derivative $\dot{\gamma}_{\text{ref}}(t)$ and of the forces exerted by the lines on the innermost control system. All these contributions are bounded, hence $w(t)$ can be seen as a bounded disturbance acting on the system. The scalar $\tilde{K}(t)$ is the only uncertain parameter in matrix A_{cl} , and it depends on several other variables. However, by exploiting Proposition 1, upper and lower limits \tilde{K}^i , $i = 1, 2$, can be easily derived on the basis of the available knowledge on the system, such that $\tilde{K} \in [\tilde{K}^1, \tilde{K}^2]$. Then, any possible matrix $A_{cl}(\tilde{K})$ results to be contained in the convex hull defined by the vertices $A_{cl}(\tilde{K}^1)$, $A_{cl}(\tilde{K}^2)$. After computing these vertices, existing results based on quadratic stability and linear matrix inequalities (LMIs) can be used to assess the robust stability of system (22). In particular, the system (22) results to be robustly stable if there exists a positive definite matrix $P = P^T \in \mathbb{R}^{3 \times 3}$ such that (e.g., [23])

$$A_{cl}^T(\tilde{K}^i)P + PA_{cl}(\tilde{K}^i) < 0, \quad i = 1, 2 \quad (23)$$

where T stands for the matrix transpose operation. Condition (23) can be easily checked by using an LMI solver. In Section IV, we show that indeed a unique value of K_c guarantees robust stability of the velocity angle control loop for a wide range of operating conditions. Since the wing's velocity can be measured quite accurately, we could also adopt a gain scheduling approach and make the gain in (21) depend on $|\vec{v}(t)|$, to improve the performance. However, in our experimental tests this was not needed, as the control system achieved satisfactory performance for all the conditions of wind speed (and, consequently, of wing speeds) that we experienced, as well as with all the three different wings we tested.

Finally we remark that, due to the physical limitations of the actuator, the position $\delta_m(t)$ is constrained in the range $\pm \bar{\delta}_m$, where $\bar{\delta}_m$ is a positive scalar. Similarly, we saturate the reference position $\delta_{m,\text{ref}}(t)$ in the same range. However, we note that these saturations are never active during operation (we show this fact with measured data in the next section), hence the stability analysis reported above is still valid even if it does not account explicitly for the input limits. Fig. 6 shows a scheme of the velocity angle controller.

C. Outer Control Loop

The outer control loop (shown in Fig. 7) is responsible for providing the velocity angle control loop with a reference heading $\gamma_{\text{ref}}(t)$. Our goal is to derive a control algorithm able to achieve figure-eight crosswind paths, with few tuning

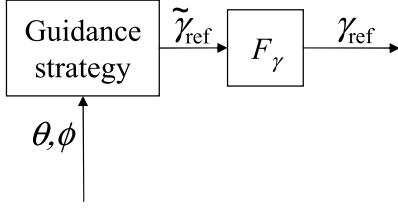


Fig. 7. Scheme of the guidance strategy.

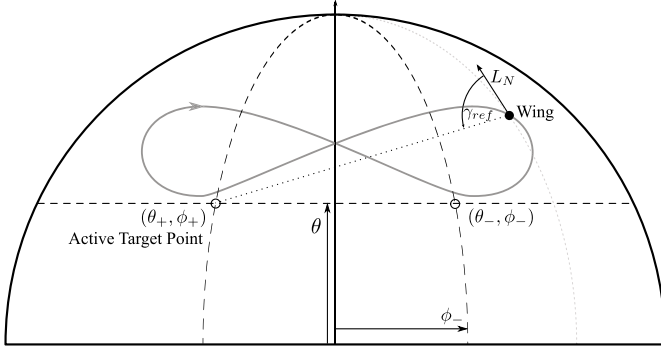


Fig. 8. Sketch of the control strategy for the outermost loop. Wind window projected on the (y, z) plane (black solid line), target points P_- , P_+ (\circ), traces of points with constant θ , and ϕ (dashed lines), example of wing's path (gray solid line), and example of how the reference γ_{ref} is computed for a given wing position (\bullet).

parameters. Hence, we want to avoid the need to precompute a whole trajectory to be used as reference, as it has been done in previous researches [8], [11]. Precomputed reference paths are based on some mathematical model of the system, with the consequent unavoidable issues of model mismatch and approximation that might give rise to problems related to stability and attractiveness of the chosen trajectory. In [17], a bang-bang-like strategy to set the reference heading of the wing, avoiding the use of precomputed reference flying paths, has been described. Here, we propose a similar approach, whose advantage is to provide an intuitive link between the tuning parameters and the position of the resulting paths in the wind window.

In our approach, we define two fixed reference points in the (ϕ, θ) plane, denoted by $P_- = (\phi_-, \theta_-)$ and $P_+ = (\phi_+, \theta_+)$, with $\phi_- < \phi_+$ (Fig. 8). The controller computes a new value of the reference velocity angle at discrete time instants. At each time step $k \in \mathbb{Z}$, one of the two reference points is set as the active target $P_a(k) = (\phi_a(k), \theta_a(k))$, according to a switching strategy that we describe next. Then, a first target velocity angle $\tilde{\gamma}_{\text{ref}}(k)$ is computed on the basis of the measured values of $\theta(k)$ and $\phi(k)$ as follows:

$$\tilde{\gamma}_{\text{ref}}(k) = \arctan \left(\frac{(\phi_a(k) - \phi(k)) \cos(\theta(k))}{\theta_a(k) - \theta(k)} \right) \quad (24)$$

i.e., to make the wing's velocity vector point toward the active target [compare the definition of $\gamma(t)$ in (12)]. Finally, the actual reference γ_{ref} is computed as the output of a second-order Butterworth filter F_γ , whose input is $\tilde{\gamma}_{\text{ref}}$, with cutoff frequency ω_γ (to be tuned by the control designer), to provide a smooth reference as input to the velocity angle control loop.

TABLE I
LUMPED PARAMETERS OF THE WINGS EMPLOYED IN THE
EXPERIMENTAL ACTIVITIES

Airush One® 12		
Area	A	12 m ²
Mass	m	2.9 kg
Wingspan	d_s	3.1 m
Equivalent aerodynamic efficiency (average)	E_{eq}	5.3
Lift coefficient (average)	C_L	0.85
Airush One® 9		
Area	A	9 m ²
Mass	m	2.45 kg
Wingspan	d_s	2.7 m
Equivalent aerodynamic efficiency (average)	E_{eq}	5.6
Lift coefficient (average)	C_L	0.8
Airush One® 6		
Area	A	6 m ²
Mass	m	1.7 kg
Wingspan	d_s	1.8 m
Equivalent aerodynamic efficiency (average)	E_{eq}	5.1
Lift coefficient (average)	C_L	0.6

The target points are switched according to the following strategy

$$\begin{aligned} \text{If } \phi(k) < \phi_- \text{ then } P_a(k) &= P_+ \\ \text{If } \phi(k) > \phi_+ \text{ then } P_a(k) &= P_- \\ \text{Else } P_a(k) &= P_a(k-1). \end{aligned} \quad (25)$$

Thus, the target point is switched when the measured value of ϕ is outside the interval $[\phi_-, \phi_+]$. By how we defined the velocity angle γ , after the target point has been switched the wing will start turning, under the action of the inner control loops, following “up-loops,” i.e., pointing first toward the zenith of the wind window and then to the other target point. The main parameters to be chosen in the described guidance strategy are the target points P_- , P_+ , which can be intuitively tuned using simplified equations of crosswind motion like those presented in [16], and the cutoff frequency ω_γ , which can be tuned to have sharper (for higher ω_γ) or wider (for smaller ω_γ) turns of the wing (we provide an example obtained from our experiments in Section IV). Finally, we note that the described approach does not rely on any measurement or estimate of the wind speed, however, the interval $[\phi_-, \phi_+]$ shall be centered around the wind direction, to make the wing fly in crosswind conditions. A rough measure of the wind direction can be obtained through standard wind vanes, in addition an estimate can be obtained from other measured quantities, such as the wing's speed and line forces, as we discuss in Section V.

IV. EXPERIMENTAL RESULTS

We present here the experimental results obtained with our small-scale prototype. The data correspond to ~ 22 h of autonomous flight time in total, i.e., ~ 14000 complete figure-eight paths. The longest flight was of 4.3 h. In all

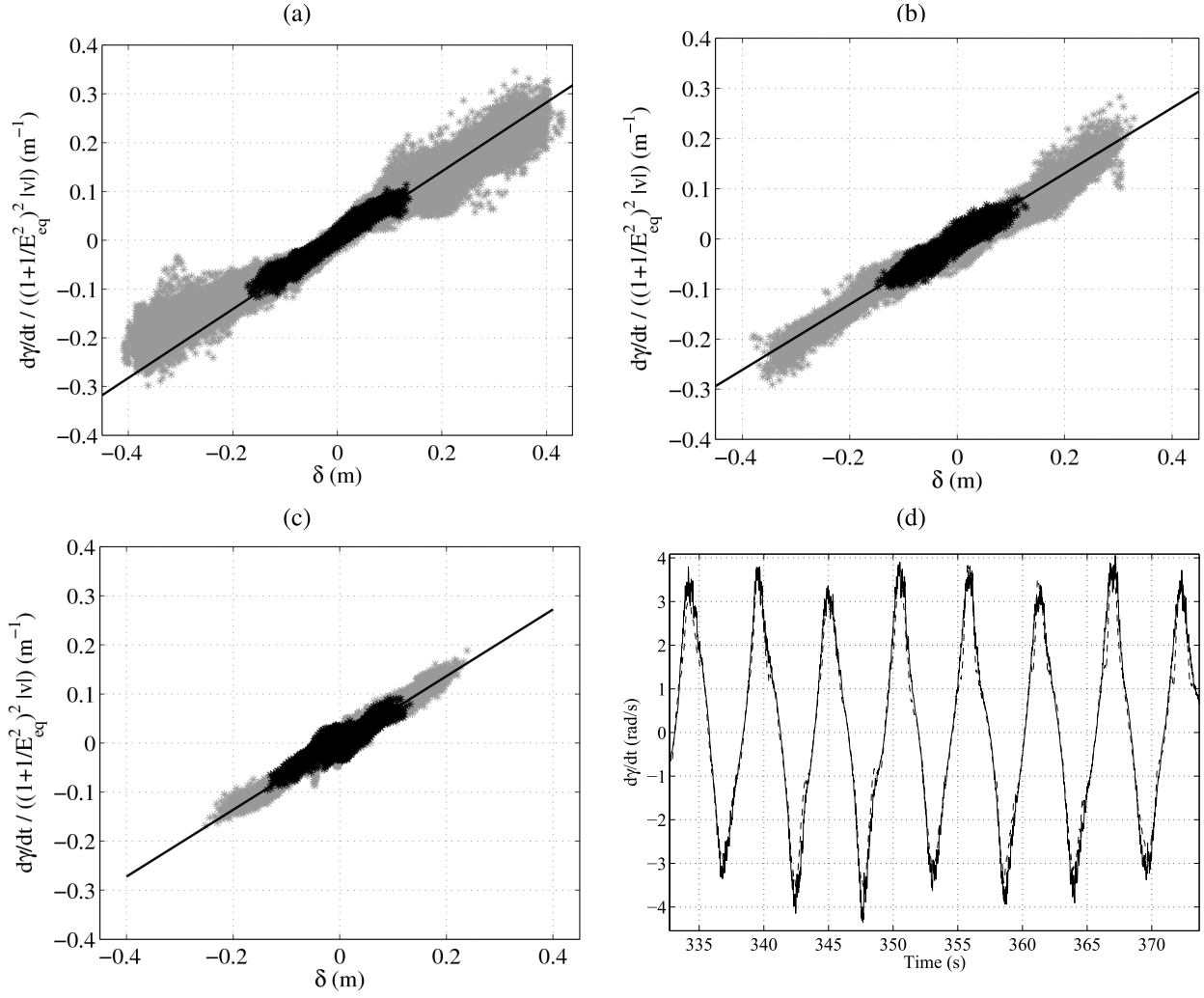


Fig. 9. Experimental results. (a)–(c) Comparison between the measured values of $\dot{\gamma}/((1+1/E_{eq}^2)^2 |\vec{v}|)$ as a function of the steering input $\delta(t)$ (gray and black dots) and the theoretical linear relationship given by the gain $\rho C_L A/2md_s$ as per (16a) (solid line). The gray dots represent experimental data collected in the whole range of θ, ϕ spanned by the wing during operation, while the black dots represent values collected when $|\phi| \leq 5^\circ$, i.e., in crosswind conditions. (a) Airush One 6 kite. (b) Airush One 9 kite. (c) Airush One 12 kite. The lumped parameters for the kites are reported in Table I. (d) Comparison between the value of $\dot{\gamma}$ obtained in experimental tests (solid) and the one estimated using the simplified model and the result of Proposition 1 (dashed line). Wing size: 6-m².

the tests, the takeoff and landing maneuvers were started and ended by a human operator. The control system was able to achieve consistently autonomous flight in different wind conditions and with three different wings. In particular, we employed a 6-, 9-, and 12-m² Airush One power kites in the tests.

We first present a comparison between the control-oriented model (15)–(16a) and the experimental data collected during the tests, and then we focus on the implementation of the control system and on the resulting performance.

A. Experimental Assessment of the Control-Oriented Model for Tethered Wings

To show the matching between Proposition 1 and the experimental evidence, we first estimate the equivalent efficiency $E_{eq}(t)$ and the lift coefficient $C_L(t)$ of each wing. To this end, we consider 10% of the data that we collected with each wing. Using this data, we obtain an estimate of the $E_{eq}(t)$

by computing the ratio between the wing speed relative to the ground, $|\vec{v}(t)|$ (which is estimated accurately using a line angle sensor and an onboard inertial measurement unit, [19] for details), and the magnitude of the absolute wind \vec{W} projected on the line direction, i.e., $|\vec{W}| \cos(\theta) \cos(\phi)$, measured with an anemometer placed at 4 m above the ground. This estimate is justified by the theoretical equations of crosswind flight (e.g., [16]), which are also valid under Assumption 1, and it is reasonable in our setup thanks to the short line length of 30 m, such that the wind could be measured at an elevation quite close to that of the wing. We remark that we used the wind measurements only for the purpose of data analysis and not as a feedback variable in the control system. As to the value of the lift coefficient $C_L(t)$, we estimate it from the following theoretical equation (e.g., [16]):

$$|\vec{F}_c(t)| = \frac{\rho C_L(t) A}{2} E_{eq}(t) \left(1 + \frac{1}{E_{eq}(t)^2}\right)^{3/2} \cdot \left(\cos(\theta(t)) \cos(\phi(t)) |\vec{W}(t)|\right)^2 \quad (26)$$

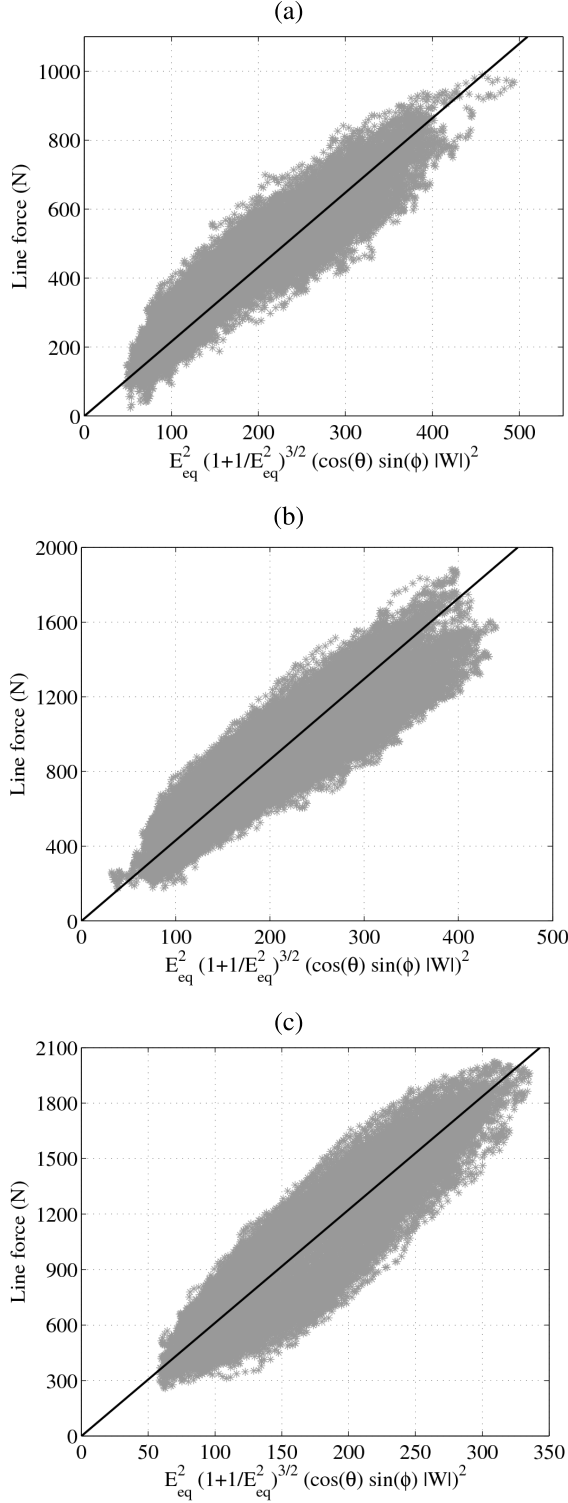


Fig. 10. Experimental results. Comparison between the measured values of total line force as a function of the quantity $E_{\text{eq}}(1 + 1/E_{\text{eq}}^2)^{3/2} (\cos \theta \cos(\phi) |\vec{W}|)^2$ (gray dots) and the theoretical linear relationship given by the gain $\rho C_L A/2$ (26). (a) Airush One 6 kite. (b) Airush One 9 kite. (c) Airush One 12 kite. The lumped parameters for the kites are reported in Table I.

where the total line force $|\vec{F}_c(t)|$ was measured with load cells installed on the GU. The estimated values of $E_{\text{eq}}(t)$ and $C_L(t)$ exhibit low variability, hence in the analysis we consider their average values E_{eq}, C_L , reported in Table I.

TABLE II
SYSTEM AND CONTROL PARAMETERS

System's parameters		
Actuator gain	K_m	0.73 m/(s A)
Actuator pole	ω_m	1.9 rad/s
Position limits	$\bar{\delta}_m$	0.35 m
Current limits	\bar{i}_m	10 A
Distance between steering lines' attachment points	d	0.5 m
Tether length	r	30 m
Gain between motor position and line lengths' difference	K_δ	4
Air density	ρ	1.2 kg/m ³
Position control loop		
Sampling frequency		100 Hz
Damping	ζ_{cl}	0.7
Natural frequency	ω_{cl}	78 rad/s
Velocity angle control loop		
Sampling frequency		50 Hz
Feedback gain	K_c	0.046 m/rad
Guidance strategy		
Sampling frequency		50 Hz
Target points	P_+, P_-	variable
Butterworth filter cutoff frequency	ω_γ	variable

The obtained values are in line with the existing knowledge of the aerodynamics of tethered curved wings: indeed, from previous researches and physical insight, values of E_{eq} in the range [4,6] and C_L in the range [0.5,1] are reasonable.

We then evaluate the quality of the control-oriented model (15)–(16) and of (26) using the remaining 90% of the data for each wing.

We first compare the measured values of $\dot{\gamma}$, normalized by $(1 + 1/E_{\text{eq}}^2)^2 |\vec{v}(t)|$, with the steering input $\delta(t)$: according to (16a), these two quantities are proportional through the gain given by $\rho C_L A/(2md_s)$. The results of this comparison are shown in Fig. 9(a)–(c), for the 6, 9, and 12-m² wings, respectively. In Fig. 9(a)–(c), the gray dots represent experimental data collected in the whole range of θ, ϕ spanned by the wing during operation, while the black dots represent values collected when $|\phi| \leq 5^\circ$, i.e., in crosswind conditions. It can be noted that the linear relationship given by the model (16a) matches quite well with the experimental data, not only in crosswind conditions, where the underlying assumptions are valid, but also with larger values of ϕ , in the range $\pm 35^\circ$. Finally, in Fig. 9(d) we show an example of the matching between the time course of $\dot{\gamma}$ during figure-eight paths with the 6-m² wing and the estimate given by the model (15)–(16). Overall, the presented results provide a bridge between the existing dynamical models of the steering behavior of tethered wings, as proposed by [11], [17], and experimental evidence.

The force (26) also shows generally a good matching with the experimental data, albeit with larger variability, as it can be seen in Fig. 10(a)–(c).

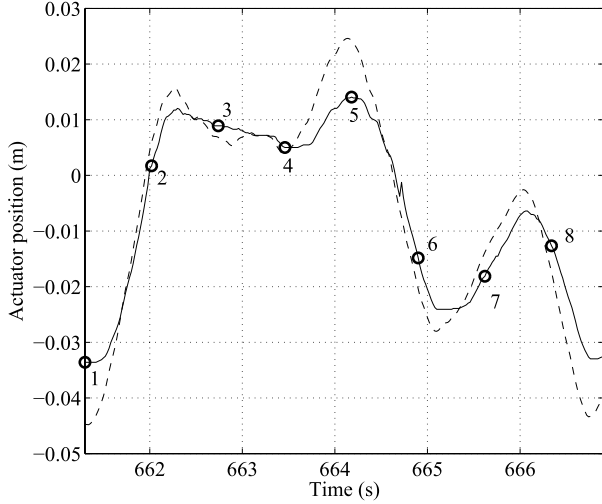


Fig. 11. Experimental results. Example of courses of target position $\delta_{m,\text{ref}}(t)$ (dashed line) and actual position $\delta_m(t)$ (solid line) of the actuator obtained with the designed innermost control loop, during automatic flight tests of a 9-m² wing. The numbered circles correspond to the conditions highlighted in Fig. 12. Guidance parameters: $\theta_+ = \theta_- = 0.35$ rad, $\phi_- = -0.2$ rad, and $\phi_+ = 0.2$ rad; $\omega_\gamma = \pi/2$ rad/s.

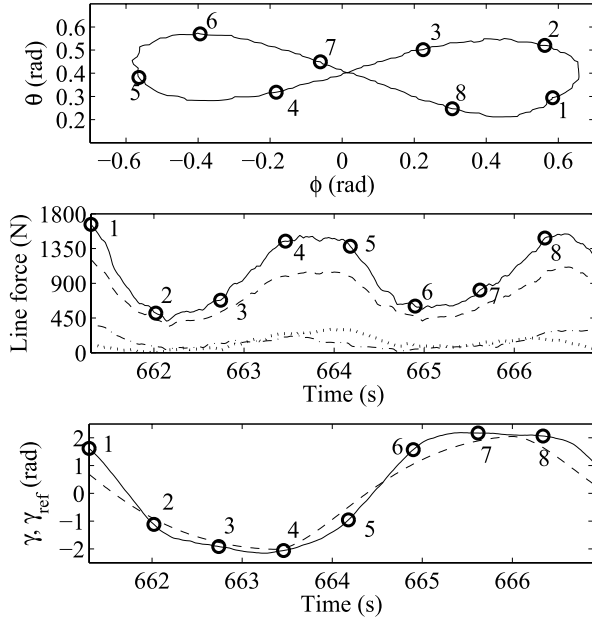


Fig. 12. Experimental results. Single figure-eight path obtained during automatic test flights with ~ 2.4 -m/s wind speed measured at 4 m above the ground. From top to bottom: flying path in (ϕ, θ) coordinates, course of the total force acting on the lines (solid line) and of the forces acting on the left (dotted), right (dash-dot), and center (dashed) lines, course of the velocity angle γ (solid line) and reference velocity angle γ_{ref} (dashed). Employed wing: 9 m². Guidance parameters: $\theta_+ = \theta_- = 0.35$ rad, $\phi_- = -0.2$ rad, and $\phi_+ = 0.2$ rad; $\omega_\gamma = \pi/2$ rad/s.

B. Controller Implementation and Experimental Results of Autonomous Flights

We implemented the controller described in Section III on a real-time machine manufactured by SpeedGoat and programmed with the xPC Target toolbox for MATLAB. The sampling frequencies we used for the control loops are 100 Hz for the innermost controller and 50 Hz for the middle and

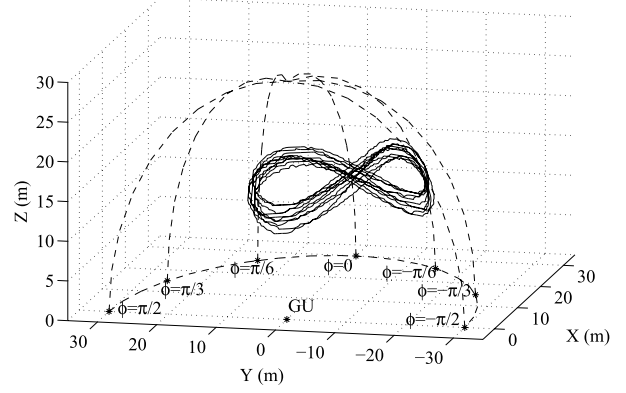


Fig. 13. Experimental results. Ten consecutive figure-eight paths in the (x, y, z) frame (solid lines), with wind misalignment. The dashed lines represent the wind window projected on the (x, y) plane as well as points with constant ϕ values and θ spanning the interval $[0, \pi/2]$. Employed wing: 9 m². Guidance parameters: $\theta_+ = \theta_- = 0.35$ rad, $\phi_- = -0.2$ rad, and $\phi_+ = 0.2$ rad; $\omega_\gamma = \pi/2$ rad/s.

outermost ones. A movie of the experimental tests is available online [24]. Table II shows the main system’s and control parameters, in addition to those reported in Table I. In Table II, the target points P_+ , P_- , and the cutoff frequency ω_γ are indicated as “variable” because we tested different values to assess the influence of these tuning parameters on the obtained performance. The first set of results that we show (Figs. 11–13) is related to the 9-m² wing; the target points’ coordinates are $\theta_+ = \theta_- = 0.35$ rad, $\phi_- = -0.2$ rad, and $\phi_+ = 0.2$ rad, and the value of ω_γ is $\pi/2$ rad/s.

Fig. 11 shows an example of the courses of $\delta_{m,\text{ref}}(t)$ and $\delta_m(t)$ obtained during the experiments with the employed controller for the innermost control loop. Note that, for the sake of simplicity, we did not include the presence of disturbances in the description of this control loop in Section III-A. Indeed the forces applied by the wing’s lines on the actuator can be modeled as an additive disturbance at this level. The effect of such disturbance can be clearly seen between points 8–1 and around point 5 in Fig. 11, where there is some error between the reference and the actual positions. By how the machine has been designed, the force exerted by each steering line on the actuator is equal to twice the force on the line. This amounts to ~ 800 N at the mentioned points in the figure. The tracking error induced by such disturbance does not influence much the performance of the overall system. If needed, the position controller can be tuned to achieve better tracking performance, at the cost of higher energy consumption. The flown path corresponding to Fig. 11 can be seen in Fig. 12, as well as the line forces and the velocity angle of the wing. To evaluate the robustness of the velocity angle control loop, we checked the condition (23) for the following ranges of the involved parameters: $|\vec{v}| \in [2, 80]$ m/s, $E_{\text{eq}} \in [2, 8]$, $C_L \in [0.4, 1]$, $A \in [6, 12]$ m², $d_s \in [1.8, 3.1]$ m, and $m \in [1.7, 3]$ kg. The considered ranges of wing speed and equivalent efficiency correspond to wind speeds in the interval $[1, 10]$ m/s, covering a wide range of normal operating conditions for airborne wind energy generators. With the considered intervals, the control system results to be stable with the chosen value of the gain

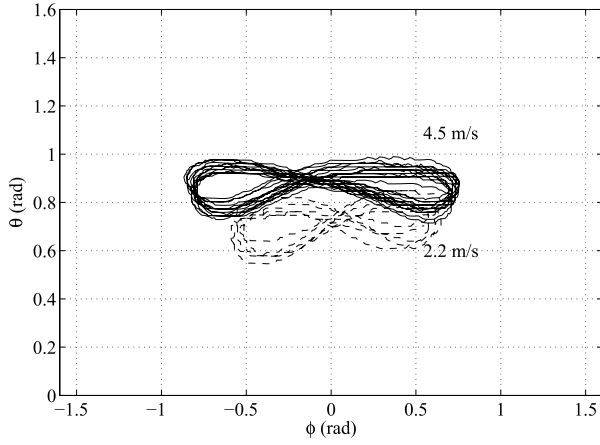


Fig. 14. Experimental results. Figure-eight paths flown with different wind speeds measured at 4 m above the ground. The solid line corresponds to a series of consecutive figure-eights flown with average wind speed of 4.5 m/s, the dashed line with average wind speed of 2.2 m/s. Employed wing: 9 m². Guidance parameters: $\theta_+ = \theta_- = 0.8$ rad, $\phi_- = -0.4$ rad, and $\phi_+ = 0.4$ rad; $\omega_\gamma = \pi/2$ rad/s.

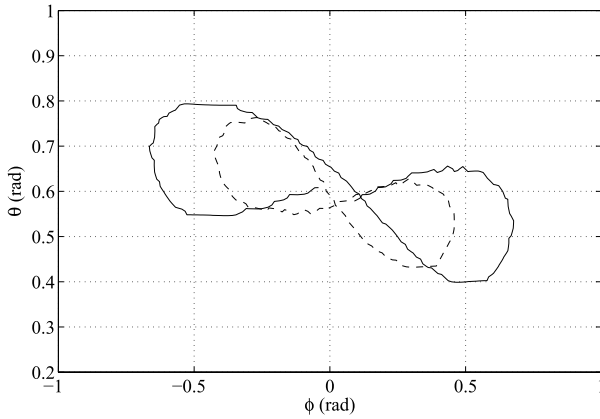


Fig. 15. Experimental results. Figure-eight paths obtained with different values of the cutoff frequency ω_γ . The solid line corresponds to $\omega_\gamma = \pi/2$ rad/s, the dashed lines to $\omega_\gamma = 2\pi$ rad/s. Employed wing: 9 m². Guidance parameters: $\theta_+ = \theta_- = 0.55$ rad, $\phi_- = -0.2$ rad, and $\phi_+ = 0.2$ rad.

$K_c = 0.046$ m/rad, thus indicating a good robustness of the approach. Indeed in our tests, the same value of K_c was used for all wind conditions and all three wings with good results. We remark that, as anticipated in Section III-B, the saturation $\bar{\delta}_m = 0.35$ m on the motor position was never active since, in practice, the commanded position is much lower, of the order of 0.05 m (Fig. 11). The wing can be effectively steered with such small values of control input thanks to the presence of the geometric input δ_g , whose effect is to contribute to steer the wing toward the center of the wind window, hence facilitating the desired up-loops figure eights. In other words, the geometric input already gives place to a “self-steering” behavior, and the aim of the controller is to apply relatively slight corrections to prevent instability and divergence of the flown paths, especially in the middle of the wind window, where the geometric input is small and the wing, without feedback control, would head straight toward the ground. This can be clearly seen by comparing the numbered

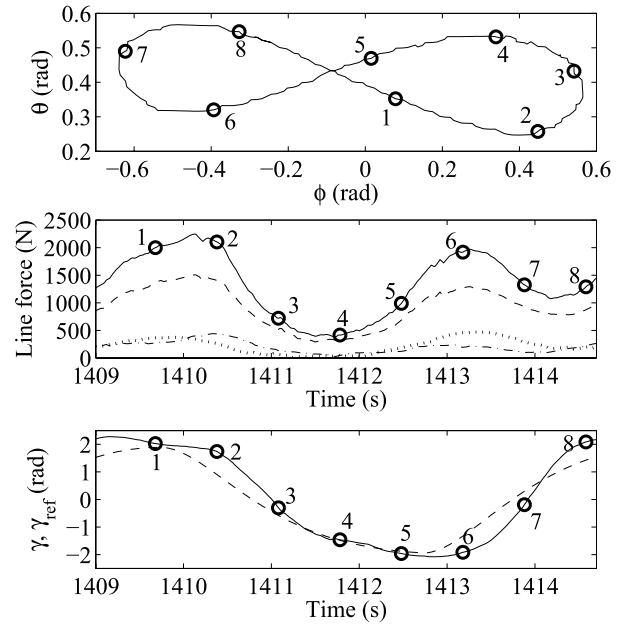


Fig. 16. Experimental results. Single figure-eight path obtained during automatic test flights with ~ 3.1 -m/s wind speed measured at 4 m above the ground. From top to bottom: flying path in (ϕ, θ) coordinates, course of the total force acting on the lines (solid line) and of the forces acting on the left (dotted), right (dash-dot), and center (dashed) lines, course of the velocity angle γ (solid line) and reference velocity angle γ_{ref} (dashed). Employed wing: 12 m². Guidance parameters: $\theta_+ = \theta_- = 0.4$ rad, $\phi_- = -0.2$ rad, and $\phi_+ = 0.2$ rad; $\omega_\gamma = \pi/2$ rad/s.

points in Figs. 11 and 12 (top). In Fig. 12 (bottom), a typical example of the courses of the reference $\gamma_{\text{ref}}(t)$ and of the actual velocity angle $\gamma(t)$ obtained during the experiments is shown, and it can be noted that the middle control loop achieves good performance in tracking the desired velocity angle. The proposed control approach has been successfully tested under various conditions. The controller was able to deal with varying wind speed from ~ 2 up to 6 m/s (measured at 4 m above the ground), achieving similar, consistent flight paths also in the presence of gusts. Wind speeds < 2 m/s would not allow the employed wings to fly without stalling, and we avoided to test with wind speeds > 6 m/s not to stress too much the wing itself, the lines and the mechanical frame, pulleys and other components of the prototype (we recall that the involved forces increase linearly with the square of the wind speed). Misalignments of the GU with respect to the wind direction up to 30° did not pose a problem for the overall control strategy. However, if the target points (and thus the figure-eight paths) are not centered with respect to the wind, the flight trajectory becomes slightly asymmetric in terms of altitude. This phenomenon can be seen in Fig. 13. Fig. 14 shows the results obtained with different wind speeds, again with the 9-m² wing and target points set to $\theta_+ = \theta_- = 0.8$ rad, $\phi_- = -0.4$ rad, and $\phi_+ = 0.4$ rad. The results of Fig. 14 highlight the fact that, since the proposed controller does not aim to track a given, specific reference path, the resulting figure-eight trajectories change with different wind conditions. However, the results also indicate that such changes are not dramatic, in addition the flown paths can be intuitively adjusted

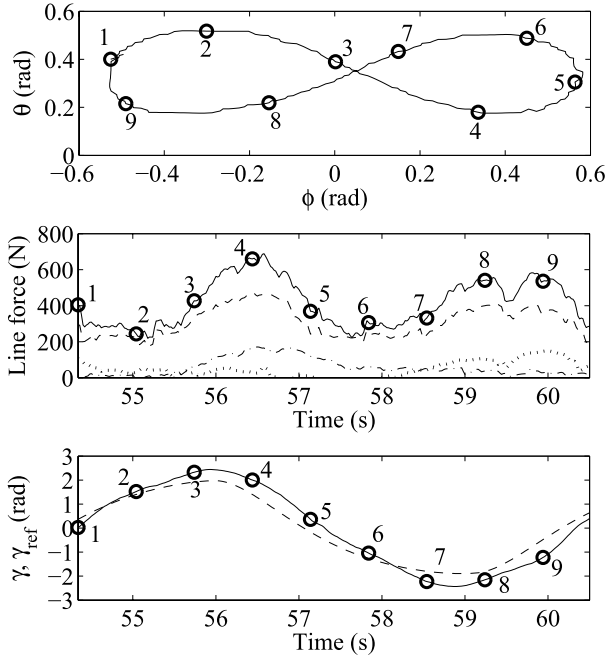


Fig. 17. Experimental results. Single figure-eight path obtained during automatic test flights with ~ 2.2 -m/s wind speed measured at 4 m above the ground. From top to bottom: flying path in (ϕ, θ) coordinates, course of the total force acting on the lines (solid line) and of the forces acting on the left (dotted), right (dashed-dotted line), and center (dashed) lines, course of the velocity angle γ (solid line) and reference velocity angle γ_{ref} (dashed line). Employed wing: 6 m^2 . Guidance parameters: $\theta_+ = \theta_- = 0.35 \text{ rad}$, $\phi_- = -0.2 \text{ rad}$, and $\phi_+ = 0.2 \text{ rad}$; $\omega_\gamma = \pi/2 \text{ rad/s}$.

by changing the position of the target points P_- , P_+ employed in our guidance strategy.

As mentioned in Section III-C, the cutoff frequency ω_γ can be used to influence the course of the reference velocity angle. The higher this frequency, the faster the transient behavior of $\gamma_{\text{ref}}(t)$ when the target point is switched, with consequent sharper turns and smaller flown paths: an example can be seen in Fig. 15, where the target points are set to $\theta_+ = \theta_- = 0.55$, $\phi_- = -0.2$, $\phi_+ = 0.2$ and two different values of ω_γ are considered. Figs. 16 and 17 show an analysis of typical figure-eight paths obtained with the 12-m^2 and with the 6-m^2 wings, respectively; while the qualitative results are similar to those obtained with the 9-m^2 wing, these figures show the quantitative differences in terms of generated forces and behavior of the velocity angle.

V. CONCLUSION

The presented experimental results indicate that the approach is able to achieve consistently and robustly figure-eight crosswind flight paths, without the need to measure or estimate neither the wind speed at the wing's altitude nor the apparent wind speed. The presence of few parameters and the intuitive guidance strategy make the approach easy to implement and tune. In addition, the theoretical analysis of the employed control-oriented model, confirmed by the comparison with experimental data, provides new insights into the dynamics of tethered wings.

It is interesting to elaborate more on the connection between the presented control approach and the operation of airborne wind energy generators, in particular with respect to the aim of generating power. In this context, different considerations can be made, depending on the available actuators and sensors.

The simplest system configuration involves the presence of generators/motors on the ground, which can be controlled to set a desired line force or line reeling speed. In such a configuration, the wing's pitch angle cannot be influenced by the control system (like in our small-scale prototype, where we used a fixed bridling configuration). Then, the wing has to be designed/configured to provide relatively constant efficiency and lift for all the expected operating conditions, and the amount of generated power depends mainly on two aspects: 1) the location where the figure-eight paths are flown relative to the wind direction at the wing's height and 2) the line reeling speed. About the first aspect, our approach can be extended to modify in real time the location of the target points, employed in the guidance strategy, to always achieve crosswind flying paths. Such adaptation can be carried out without using a direct measure of the absolute wind direction at the wing's location (which would be not trivial to obtain), but relying on other available measurements, like the line force or the wing speed relative to the ground. In particular, misalignments with respect to the wind direction can be detected by observing the difference of line force (or wing speed) between the left and the right halves of the flown figure-eight paths. This is a topic of ongoing research and the first results are promising [25]. Regarding the second aspect for optimal power generation, i.e., the line reeling speed, the problem of controlling and optimizing this variable can be treated separately from the problem of achieving figure-eight paths. Since the generated power during the traction phase is measured and it is a concave function of the line reeling speed (e.g., [16]), its maximum value can be tracked using real-time optimization techniques, again without the need to measure the wind speed. The control system for the line reeling can then be designed independently from the crosswind flight controller. If needed, the potential interaction between the two control systems, given by the fact that the line reeling speed influences the wing's tangential velocity and hence its turning rate, can be dealt with by scheduling the gain of the velocity angle controller (21) with the wing's speed tangent to the wind window.

A more complex system configuration involves the presence of a pitch actuator in addition to the ground generators. Also in this case, the approach presented in this paper can be used without significant modifications to achieve figure-eight crosswind paths, and the control system can then modulate the line force and the wing pitch to optimize the generated power, by tracking both the optimum reel-out speed and the maximum lift/drag ratio. This can be done by exploiting either existing measurements, such as line forces and wing speed, or additional ones, such as the onboard airflow.

In summary, the control problem for the traction phase of ground-based airborne wind energy generators involves two objectives, i.e., the stabilization of the figure-eight trajectories and the optimization of the generated power, and two or

three input variables, depending on the available actuators. The approach presented in this paper exploits one of such input variables (i.e., the steering deviation) to achieve the first control objective, hence decoupling it from the second one, which can then be tackled by exploiting the other inputs (i.e., the line force and, eventually, the wing pitch), through additional feedback strategies that can be straightforwardly combined or integrated in the control system.

The natural development of this research will be the execution of full generating cycles with the considered concept of airborne wind generator, and the comparison of the obtained results with the existing theoretical and numerical analyzes. To this end, we are currently investigating the extension of the presented technique to adapt to varying wind direction, the design of a control approach able to address the problem of optimal line reel-out, finally the design of a strategy to optimize the passive (i.e., retraction) phase of the generator.

APPENDIX

PROOF OF PROPOSITION 1

For the sake of simplicity of notation, in the following we drop the dependance of time-varying variables from t . We start by deriving an analytic expression for the velocity angle rate. For this we take the derivative of (12) to obtain

$$\dot{\gamma} = \frac{\cos(\theta)\dot{\theta}\ddot{\phi} - \sin(\theta)\dot{\phi}\ddot{\theta} - \cos(\theta)\dot{\phi}\ddot{\theta}}{\cos(\theta)^2\dot{\phi}^2 + \dot{\theta}^2}. \quad (27)$$

The accelerations $\ddot{\theta}$ and $\ddot{\phi}$ in (27) can be expressed as functions of the forces acting on the wing using the model equations (2)–(11). By Assumption 1, neglecting all forces except for the aerodynamic ones and considering the balance of the lift and drag forces in the direction of the wing velocity \vec{v} , we have (e.g., [16])

$$\frac{\sin(\Delta\alpha)}{\cos(\Delta\alpha)} = \frac{1}{E_{\text{eq}}} \doteq \frac{C_{D,\text{eq}}}{C_L} \quad (28)$$

where E_{eq} is the equivalent efficiency of the wing. From the equation above, we can see that $\Delta\alpha$ is small for a reasonable wing efficiency of 4–6. Measurements of test flights have shown that $\Delta\alpha < 0.3$ rad, and most of times $\Delta\alpha < 0.2$ rad. Therefore, we can linearize (28) to obtain

$$\Delta\alpha = \frac{1}{E_{\text{eq}}}. \quad (29)$$

In addition, on the basis of Assumption 2 we can simplify also η in (9) as $\eta = \Delta\alpha\psi$. Finally, by Assumption 1 the component of absolute wind perpendicular to the tether is zero, and the velocity angle $\gamma \simeq \xi$. Hence, the aerodynamic force components given by (7) and (8) can be simplified as follows:

$$\begin{aligned} {}_L\vec{F}_a &= \frac{1}{2}\rho C_L A |\vec{W}_a|^2 \begin{pmatrix} \Delta\alpha \cos(\gamma) - (\Delta\alpha^2\psi + \psi) \sin(\gamma) \\ \Delta\alpha \sin(\gamma) + (\Delta\alpha^2\psi + \psi) \cos(\gamma) \\ -1 \end{pmatrix} \\ &+ \frac{1}{2}\rho C_{D,\text{eq}} A |\vec{W}_a|^2 \begin{pmatrix} \cos(\gamma) \\ -\sin(\gamma) \\ -\Delta\alpha \end{pmatrix}. \end{aligned} \quad (30)$$

Using (27) and (2)–(3) with (30) we obtain

$$\begin{aligned} \dot{\gamma} &= \frac{\frac{1}{2}\rho C_L A |\vec{W}_a|^2 \dot{\theta} \cos(\gamma) + \cos(\theta)\dot{\phi} \sin(\gamma)}{r m \cos(\theta)^2\dot{\phi}^2 + \dot{\theta}^2} (\Delta\alpha^2 + 1) \psi \\ &+ \frac{\frac{1}{2}\rho A |\vec{W}_a|^2 (C_L \Delta\alpha - C_{D,\text{eq}}) (\dot{\theta} \sin(\gamma) - \cos(\theta)\dot{\phi} \cos(\gamma))}{r m \cos(\theta)^2\dot{\phi}^2 + \dot{\theta}^2} \\ &+ \frac{r m \sin(\theta)\dot{\phi} (\dot{\theta}^2 + \cos(\theta)^2\dot{\phi}^2)}{r m \cos(\theta)^2\dot{\phi}^2 + \dot{\theta}^2} + \frac{g \cos(\theta)^2\dot{\phi}}{r (\cos(\theta)^2\dot{\phi}^2 + \dot{\theta}^2)}. \end{aligned} \quad (31)$$

Following the same argument by which (29) is derived, we also obtain:

$$|\vec{W}_a(t)|^2 \simeq \left(1 + \frac{1}{E_{\text{eq}}^2}\right)^2 |\vec{v}|^2. \quad (32)$$

Considering (6), $|\vec{v}|$ is computed as

$$|\vec{v}| = \sqrt{r^2 (\cos(\theta)^2\dot{\phi}^2 + \dot{\theta}^2)} \quad (33)$$

which is, by the definition of γ (12), also equal to

$$|\vec{v}| = r\dot{\theta} \cos(\gamma) + r \cos(\theta)\dot{\phi} \sin(\gamma). \quad (34)$$

Finally, by combining (31) with (29) and (32)–(34), and considering the linearization of (10) by Assumption 2, we obtain our result

$$\dot{\gamma} = \frac{C_L \rho A}{2 m d_s} \left(1 + \frac{1}{E_{\text{eq}}^2}\right)^2 |\vec{v}| \delta + \frac{g \cos(\theta) \sin(\gamma)}{|\vec{v}|} + \sin(\theta)\dot{\phi}.$$

ACKNOWLEDGMENT

The authors acknowledge SpeedGoat's Greengoat program.

REFERENCES

- [1] Makani Power Inc. (2013, Sep.). Alameda, CA, USA [Online]. Available: <http://www.makanipower.com>
- [2] SkySails GmbH & Co. (2010). Hamburg, Germany [Online]. Available: <http://www.skysails.info>
- [3] Ampyx Power. (2013, Sep.). The Hague, The Netherlands [Online]. Available: <http://www.ampyxpower.com/>
- [4] Wind Lift. Emden, Germany [Online]. Available: <http://www.windlift.com/>
- [5] Kitenergy. Turin, Italy [Online]. Available: <http://www.kitenergy.net/>
- [6] Enerkite GmbH. Berlin, Germany [Online]. Available: <http://www.enerkite.com/>
- [7] M. Canale, L. Fagiano, and M. Milanese, "Power kites for wind energy generation," *IEEE Control Syst. Mag.*, vol. 27, no. 6, pp. 25–38, Dec. 2007.
- [8] A. Ilzhöfer, B. Houska, and M. Diehl, "Nonlinear MPC of kites under varying wind conditions for a new class of large-scale wind power generators," *Int. J. Robust Nonlinear Control*, vol. 17, no. 17, pp. 1590–1599, 2007.
- [9] M. Canale, L. Fagiano, and M. Milanese, "High altitude wind energy generation using controlled power kites," *IEEE Trans. Control Syst. Technol.*, vol. 18, no. 2, pp. 279–293, Mar. 2010.
- [10] E. Terink, J. Breukels, R. Schmehl, and W. Ockels, "Flight dynamics and stability of a tethered inflatable kiteplane," *AIAA J. Aircraft*, vol. 48, no. 2, pp. 503–513, 2011.
- [11] J. H. Baayen and W. J. Ockels, "Tracking control with adaption of kites," *IET Control Theory Appl.*, vol. 6, no. 2, pp. 182–191, 2012.
- [12] C. Vermillion, T. Grunnagle, and I. Kolmanovsky, "Modeling and control design for a prototype lighter-than-air wind energy system," in *Proc. ACC*, Jun. 2012, pp. 5813–5818.
- [13] L. Fagiano and M. Milanese, "Airborne wind energy: An overview," in *Proc. ACC*, Montreal, QC, Canada, 2012, pp. 3132–3143.

- [14] M. L. Loyd, "Crosswind kite power," *J. Energy*, vol. 4, no. 3, pp. 106–111, 1980.
- [15] P. Williams, B. Lansdorp, and W. Ockels, "Optimal crosswind towing and power generation with tethered kites," *J. Guid., Control, Dyn.*, vol. 31, no. 1, pp. 81–93, 2008.
- [16] L. Fagiano, M. Milanese, and D. Piga, "Optimization of airborne wind energy generators," *Int. J. Robust Nonlinear Control*, vol. 22, no. 18, pp. 2055–2083, 2011.
- [17] M. Erhard and H. Strauch, "Control of towing kites for seagoing vessels," *IEEE Trans. Control Syst. Technol.*, vol. 21, no. 5, pp. 1629–1640, Sep. 2013.
- [18] L. Fagiano, "Control of tethered airfoils for high–altitude wind energy generation," Ph.D. dissertation, Dept. Control Comput. Eng., Politecnico di Torino, Torino, Italy, Feb. 2009.
- [19] L. Fagiano, K. Huynh, B. Bamieh, and M. Khammash, "On sensor fusion for airborne wind energy systems," *IEEE Trans. Control Syst. Technol.* [Online]. Available: <http://dx.doi.org/10.1109/TCST.2013.2269865>
- [20] L. Fagiano, M. Milanese, and D. Piga, "High-altitude wind power generation," *IEEE Trans. Energy Convers.*, vol. 25, no. 1, pp. 168–180, Mar. 2010.
- [21] I. Argatov, P. Rautakorpi, and R. Silvennoinen, "Estimation of the mechanical energy output of the kite wind generator," *Renew. Energy*, vol. 34, no. 6, p. 1525–1532, 2009.
- [22] S. Skogestad and I. Postlethwaite, *Multivariable Feedback Control*, 2nd ed. New York, NY, USA: Wiley, 2005.
- [23] F. Amato, "Quadratic stability," in *Robust Control of Linear Systems Subject to Uncertain Time-Varying Parameters* (Lecture Notes in Control and Information Sciences), vol. 325. Berlin Heidelberg: Springer-Verlag, 2006, pp. 31–92.
- [24] (2012, Sep.). *Autonomous Flexible Wings for High-Altitude Wind Energy Generation* [Online]. Available: <http://youtu.be/2ek65AiIkqM>
- [25] A. U. Zraggen, L. Fagiano, and M. Morari, "On real-time optimization of airborne wind energy generators," in *Proc. IEEE CDC*, Firenze, Italy, Dec. 2013.